REVIEW

Electronic structure in the transition metal block and its implications for light harvesting

James K. McCusker

Transition metal–based chromophores play a central role in a variety of light-enabled chemical processes ranging from artificial solar energy conversion to photoredox catalysis. The most commonly used compounds include elements from the second and third transition series (e.g., ruthenium and iridium), but their Earth-abundant first-row analogs fail to engage in photoinduced electron transfer chemistry despite having virtually identical absorptive properties. This disparate behavior stems from fundamental differences in the nature of 3d versus 4d and 5d orbitals, resulting in an inversion in the compounds' excited-state electronic structure and undermining the ability of compounds with first-row elements to engage in photoinduced electron transfer. This Review will survey the key experimental observations establishing this difference in behavior, discuss the underlying reasons for this phenomenon, and briefly summarize efforts that are currently under way to alter this paradigm and open the door to new opportunities for using Earth-abundant materials for photoinduced electron transfer chemistries.

The conversion of light to chemical energy is the basis of photosynthesis, in which light absorption results in a separation of charge that creates the chemical potential needed to drive biochemical synthesis with adenosine triphosphate (ATP) as an energy carrier. The effective capture and use of sunlight, an inexhaustible, globally accessible, and pollution-free energy source, is critical for replacing fossil fuels to mitigate global climate change (*1*). Whereas nature uses solar energy to create chemical fuels, artificial systems have focused largely on electrical generation. The recent drop in the cost of silicon has led to a marked increase in the amount of installed solar capacity (*2*), but the intermittent nature of solar energy, the balance of systems costs that continues to represent a substantial economic obstacle (*3*), and the fact that electricity constitutes only ~30% of the global energy footprint (*4*) underscore the need for continued research on strategies for converting solar energy to fuels.

An artificial molecular system for replicating photosynthesis must do what photosynthetic systems do—that is, use the energy of a photon to spatially separate charges and thereby create a chemical potential. This represents the thermodynamic part of the problem, but kinetics also play an important role. Specifically, the photoexcited state must have a lifetime sufficiently long such that the resulting chemical potential can be used to drive a reaction before that potential is lost to unproductive competing pathways (e.g., charge recombination). The combination of these thermodynamic and kinetic requirements, coupled with the scale of fuel generation required to affect the use of fossil fuels, is where the periodic properties of the transition metals come into play.

Department of Chemistry, Michigan State University, East Lansing, MI 48824, USA. Email: jkm@chemistry.msu.edu

Photoinduced charge transfer between metals and ligands

In molecular approaches to photoinduced electron transfer chemistry, the excited state created upon the absorption of light must be "redox active" in the sense that it can engage in chemical reactions in which a substrate interacting with the chromophore can be reduced and/or oxidized. Transition metal–based chromophores are particularly well suited for such applications because most have so-called charge-transfer excited states. A metal-to-ligand charge-transfer (MLCT) state, for example, uses a photon to redistribute charge within the molecule by transferring an electron from a nominally metal-centered orbital to one associated with the ligand. This process is paramount to a photoinduced oxidation of the metal and concomitant reduction of the ligand and provides the means for the metal to act as an electron acceptor and the ligand as an electron donor; ligand-to-metal charge-transfer (LMCT) states reverse these roles but achieve the same end result, photoinduced charge separation. With proper design, the electron transfer processes subsequent to light absorption release energy. In this regard, one can view sunlight as the energy input that pushes an otherwise thermodynamically unfavorable reaction uphill, much the same way as in the initial steps of photosynthesis.

A primary reason for needing Earth-abundant metals for molecular chromophores is that the solar photon flux is ~100 mW cm^{-2}. This presents a very small cross section for light absorption and makes this part of the solar energy conversion process material-intensive (photosynthesis operates under this same flux, and trees have many leaves for that reason). Unfortunately, the types of compounds for which the charge-transfer states described previously are sufficiently long-lived to effect photoinduced electron transfer contain some of the rarest elements on Earth. $[Ru(bpy)_3]^{2+}$, for example (where bpy is 2,2′-bipyridine) (Fig. 1), represents a prototypical MLCT chromophore: This compound and related derivatives have been successfully used in countless research settings ranging from dye-sensitized solar cells (*5*) to photoredox catalysis (*6*). Although the chemistry associated with these excited states fulfills all of the necessary criteria, ruthenium is one of the five or six least abundant elements in Earth's crust and is simply not a viable option as the light-harvesting component for a globally scaled problem like solar fuel production.

An obvious alternative is to use chromophores containing Earth-abundant materials. For transition metal–based approaches, this means developing photoredox-active chromophores with first-row metals. However, the literature on inorganic photophysics includes few examples in which first-row metal complexes have been successfully used in chemical transformations reliant on photoinduced charge-transfer reactivity in a manner similar to what is observed in the second and third transition series. Compounds that incorporate Fe(II) provide a convenient basis for comparison because they are isoelectronic with Ru(II). In 1998, Ferrere and Gregg described a dye-sensitized solar cell fabricated by using an Fe(II)-based polypyridyl complex as the chromophore (*7*), but despite being the first functional cell incorporating Fe(II), its measured efficiency was $^1/_{100}$ the ~10% efficiency achieved by Ru(II)-based cells at that time. Although a number of factors determine the overall performance of these devices, the incident photo-to-current efficiency of the Fe-based cell clearly shows that one major factor is a reduction in the number of charge carriers (i.e., electrons) that are transferred to the semiconductor substrate after light absorption by the chromophore. So why does charge separation after light capture appear to vanish upon shifting just one row up in the periodic table?

Excited-state ordering and the primogenic effect

The phenomenological origin of the failure of an Fe(II)-based chromophore to effect charge

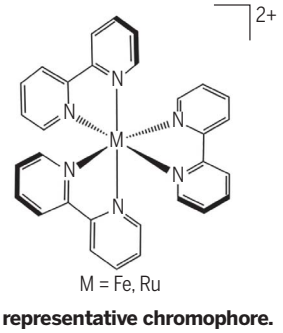

Fig. 1. A representative chromophore. Schematic representation of a transition metal–based tris-(2,2′-bipyridine) complex (e.g., $[Ru(bpy)_3]^{2+}$).

separation was first intimated in 1980 (*8*). Characterization of a charge-transfer excited state is generally achieved through the use of time-resolved absorption spectroscopy. An MLCT state, for example, can be thought of as a photo-induced redox process in which an electron in a molecular orbital predominantly metal in character is transferred to an orbital predominantly ligand in character. For a compound such as $[Ru(bpy)_3]^{2+}$, this process can be depicted as in Eq. 1:

$$[Ru^{II}(bpy)_3]^{2+} \xrightarrow[h\nu]{} [Ru^{III}(bpy^-)(bpy)_2] \quad (1)$$

[where $h\nu$ (Planck's constant h times frequency ν) indicates excitation by light]. The observation of absorption features associated with the ligand radical anion, which can be determined a priori from spectroelectrochemical measurements (*9*), is a reliable marker for the presence of the MLCT excited state. By using picosecond time-resolved absorption spectroscopy, it was found that this characteristic feature formed for both $[Ru(bpy)_3]^{2+}$ and $[Os(bpy)_3]^{2+}$ in solution within the time resolution of their instrument (~10 ps) and subsequently decayed concomitant with ground-state recovery (~900 and ~25 ns, respectively).

By contrast, no such signal was observed when the identical experiment was performed on $[Fe(bpy)_3]^{2+}$. This difference suggests that despite the initial excitation being MLCT in nature, the charge-transfer excited state of $[Fe(bpy)_3]^{2+}$ had a lifetime of <10 ps. This upper limit was further reduced through the work of McCusker, Hendrickson, and co-workers to <1 ps in 1993 (*10*). Definitive characterization of the ultrafast nature of MLCT deactivation in Fe(II) polypyridyl complexes was reported in 2000 by Monat and McCusker (*11*), who measured the formation and subsequent decay of the MLCT excited state of $[Fe(tren(py)_3)]^{2+}$ [where tren$(py)_3$ is the condensation product between 2-pyridinecarboxaldehyde and tris(2-aminoethyl)amine] by direct observation (Fig. 2). Subsequent studies of a number of Fe(II) complexes, including $[Fe(bpy)_3]^{2+}$, have revealed that the MLCT excited-state lifetimes of this class of chromophores are generally on the order of 100 fs. This reduction in the lifetime of the MLCT excited state to one-millionth that for Ru(II) complexes is truly notable given that these two systems are isoelectronic. The short lifetimes of the charge-transfer states of these first-row metal complexes are why light absorption by these compounds cannot be easily leveraged for applications requiring charge transfer: The lifetimes are typically too short to be kinetically competent to engage in photoinduced electron transfer. This fundamental shift in excited-state dynamics manifests in other elements of the first transition series and effectively eliminates the use of many of the most abundant elements of the d-block as light-harvesting components for applications that rely on charge separation after photon capture. A review by Wenger provides a survey of recent literature related to this topic (*12*).

Studies by various groups have now established that the lowest-energy excited state of compounds such as $[Fe(bpy)_3]^{2+}$ is ligand field as opposed to charge transfer in nature. Specifically, the high-spin, metal-centered $^5T_2$ state (where T_2 refers to the symmetry and 5 reflects spin multiplicity), which is characterized by a substantial (~0.2-Å) elongation of the metal-ligand bonds and a concomitant increase in molecular volume on the order of 20 to 25 $cm^3\ M^{-1}$, has been identified from time-resolved extended x-ray absorption fine-structure studies (*13*), as well as several other x-ray (*14*), optical (*15*), and vibrational (*16*) methods. Although this state can persist for several tens of nanoseconds in a room-temperature solution, the nature of this excited state is best thought of as a rearrangement of the valence electrons among the d orbitals of the metal center relative to the ground state. There is no charge separation associated with this excited-state configuration, so its reactivity is fundamentally different from that of the MLCT excited states constituting the lowest-energy excited states of compounds such as $[Ru(bpy)_3]^{2+}$, $[Os(bpy)_3]^{2+}$, and $Ir(ppy)_3$.

Because these metal ions are isoelectronic with regard to their valence configurations, the same electronic states are present in all of these systems. The difference lies in the relative ordering of the charge-transfer and ligand-field manifolds and arises because of a phenomenon that can be traced back to fundamental aspects of atomic structure, specifically the presence (or absence) of radial nodes in the wave functions of the d orbitals. Perhaps the best discussion of what Pyykkö (*17*) dubbed the "primogenic effect" [so named because of the presence or absence of primogenic electron repulsion between core and valence electrons (see below)] was provided by Kaupp in 2007 (*18*). Whenever a shell of a given orbital angular momentum quantum number l is first occupied (1s, 2p, 3d, etc.), the Schrödinger equation dictates that these orbitals will have a single radial node at $r = 0$, that is, at the nucleus; subsequent shells for the same value of l (2s, 3p, 4d, etc.) will possess $(n - l - 1)$ radial nodes (where n is the principal quantum number) at $r \neq 0$ (1 for 4d, 2 for 5d, etc.). The consequence of this is evident from plots of the radial distribution functions of the orbitals in question (Fig. 3). It can be seen that the distance corresponding to the maximum probability amplitude of the 3d orbital is actually comparable to those for the 3s and 3p orbitals. In contrast, the 4d orbitals extend beyond the 4s and 4p orbitals. This contraction of the 3d orbitals arises because of inefficient shielding of the nuclear charge by the core electrons, an effect that is caused in large part by the absence of a radial node away from the nucleus for the $n = 3$, $l = 2$ wave function. Maximizing overlap between the 3d orbitals and an incoming ligand thus requires a relatively short metal-ligand distance, but electrostatic repulsion between the ligand and metal core electrons prevents a short bond from forming. Orbital overlap is therefore attenuated, resulting in a weakening of the metal-ligand bonds. The chemical consequence of this effect is pervasive for the first transition series and is responsible for increased ligand lability, the potential for paramagnetism in even-spin compounds, and even the color of many gemstones, all of which can be traced to the reduction in ligand-field strength endemic to first-row metal complexes relative to their second- and third-row counterparts.

Ligand-field versus charge-transfer state energetics

The consequence of the primogenic effect as it relates to light capture and conversion can be summarized in the context of a Tanabe-Sugano diagram (Fig. 4). This diagram depicts the energies of all of the ligand-field states that arise because of electron-electron repulsion within the d-orbital manifold for a given valence electron configuration. These so-called term states are designated according to their symmetry properties, where A, E, and T correspond to one-, two-,

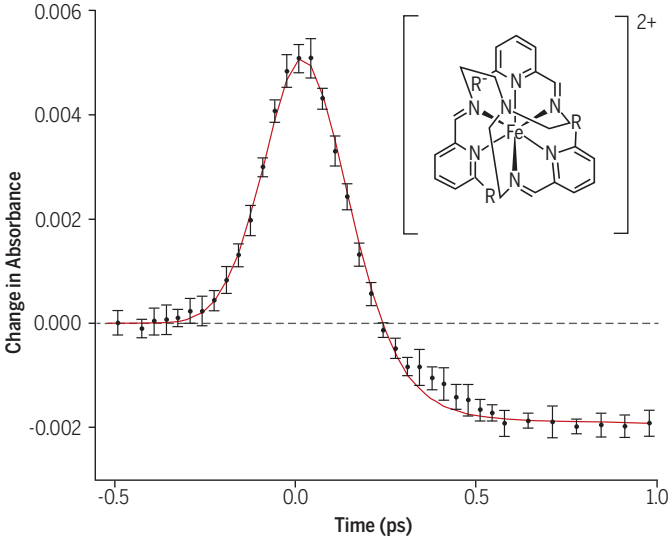

Fig. 2. First-row lifetimes. Time-resolved absorption data for an Fe(II) polypyridyl complex subsequent to MLCT excitation. The change in the sign of the signal from positive to negative is indicative of a conversion from the charge-transfer to ligand-field manifold. The solid line corresponds to fit of the data to a kinetic model indicating a lifetime of $\tau = 80 \pm 20$ fs for the MLCT state. Error bars indicate SD. R corresponds to a proton. [Adapted with permission from (*11*); copyright 2000 American Chemical Society]

and three-fold degenerate energy levels, respectively, all plotted as a function of ligand-field strength (given by Δ_O). For d^4 – d^7 configurations, the splitting between the three-fold degenerate π-symmetry t_{2g} set (i.e., d_{xy}, d_{yz}, and d_{xz}) and the formally σ antibonding e_g orbitals ($d_{x^2-y^2}$ and d_{z^2}) competes with the energy cost of placing two electrons in the same orbital (designated by the spin-pairing energy P). This leads to the possibility of having "high-spin" compounds for which Hund's rule applies, versus "low-spin" compounds where spin-pairing will occur. The crossover point (that is, where $|\Delta_O| = |P|$) is indicated in the Tanabe-Sugano diagram by the vertical line in the center and represents a demarcation between so-called weak-field ($|\Delta_O| < |P|$) and strong-field ($|\Delta_O| > |P|$) ligands that produce high-spin and low-spin compounds, respectively.

Ligands such as 2,2′-bipyridine have empty orbitals that are relatively low in energy and of the appropriate symmetry to interact with the metal-based t_{2g} orbitals. This allows for mixing between these sets of orbitals, stabilizes the resulting molecular orbital, and increases Δ_O. The same features that create this scenario also tend to produce charge-transfer transitions that lie in the visible region of the spectrum, making them well suited for light harvesting. Thus, compounds such as $[Fe(bpy)_3]^{2+}$ and $[Ru(bpy)_3]^{2+}$ are low spin and absorb strongly in the visible region.

Where the primogenic effect comes into play is in the relative positions of these two representative chromophores when projected along the x axis of Fig. 4. The presence of the radial nodes in the 4d and 5d orbitals pushes their maximum amplitudes far enough away from the nucleus to allow for strong metal-ligand overlap. The consequent splitting between the t_{2g} and e_g orbitals is characterized by a large value for Δ_O and thus positions complexes such as $[Ru(bpy)_3]^{2+}$ far to the right on the d^6 Tanabe-Sugano diagram. In contrast, the (relative) contraction of the 3d orbitals attenuates metal-ligand overlap and leads to a markedly weaker ligand field. Although the ligand field created is still strong enough to yield a low-spin compound, a compound such as $[Fe(bpy)_3]^{2+}$ will be situated well to the left of $[Ru(bpy)_3]^{2+}$ in Fig. 4. The last piece of this puzzle concerns where the charge-transfer state energy fits into this picture. Whereas ligand-field state energies are highly dependent on the strength of the metal-ligand interaction, charge-transfer states are much more strongly correlated with the redox properties of the metal and ligand (as suggested by Eq. 1). Because of this, the energy of an MLCT state will not track the magnitude of Δ_O and is therefore best represented as a line having zero slope when projected on a Tanabe-Sugano diagram, as shown in Fig. 4.

The reason for the disparate photophysical properties of $[Ru(bpy)_3]^{2+}$ and $[Fe(bpy)_3]^{2+}$ now becomes clear. Being isoelectronic, the compounds have the same array of electronic excited states, but the reduction in ligand-field splitting endemic to the first transition series coupled with roughly similar redox potentials leads to an inversion in the relative energies of the MLCT and ligand-field excited states. This is illustrated in Fig. 5, which takes the electronic states intercepted by the vertical lines for both compounds in Fig. 4 and represents them as potential energy surfaces. Photoexcitation of both compounds in the visible region results in the formation of a ^{1}MLCT excited state. In the case of $[Ru(bpy)_3]^{2+}$, a highly efficient intersystem-crossing process follows, leading to the formation of the ^{3}MLCT state that persists long enough to leverage the chemical potential stored in this charge-separated state. The metal-centered ligand-field states are present, but the larger ligand-field splitting places them at higher energy, and they are therefore not kinetically relevant. For $[Fe(bpy)_3]^{2+}$, however, this same ^{1}MLCT state is subject to excited-state dynamics not present in $[Ru(bpy)_3]^{2+}$ because the ligand-field excited states are now lower in energy. This opens up the possibility of rapid, nonradiative relaxation processes that serve as deactivation pathways for the MLCT state(s). Although they do not contribute substantially to the overall absorption cross section of the compound, they dominate the excited-state dynamics that occur subsequent to light capture and undermine the ability to use such compounds for any application where photoinduced charge separation is required.

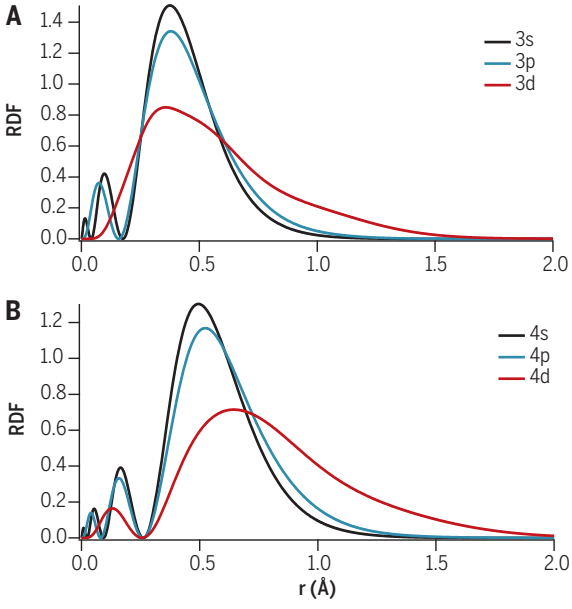

Fig. 3. The primogenic effect. Radial distribution functions (RDFs) for the $n = 3$ shell of Fe(II) (**A**) and the $n = 4$ shell of Ru(II) (**B**). The plots illustrate the consequence of the primogenic effect, wherein the lack of a radial node for $r \neq 0$ in the 3d orbital results in a contraction of that orbital, leading to weaker metal-ligand interactions than are present in the case of 4d [and 5d (not shown)] orbitals.

This discussion has focused primarily on comparisons across group 8 because the fundamental issues at play are most easily illustrated in an isoelectronic setting, but similar issues arise for other elements and oxidation states across the first transition series. That stated, there are exceptions to the general circumstances just described. Perhaps the most notable outlier is Cu(I). Chromophores with this metal ion are in fact being used in a variety of applications, including photoredox catalysis (*19*) and dye-sensitized solar cells (*20*). A primary reason why this is a notable case is now quite clear given the origin of the problem just described: Cu(I) has a d^{10} valence configuration. Because the d subshell is completely filled, no excited ligand-field states are present for complexes of this ion. Thus, the lowest-energy excited state of $[Cu(bpy)_2]^+$, for example, is MLCT in nature because the valence configuration does not provide for the existence of any other metal-based electronic excited states [this will also be true for d^0 metal complexes, such as Ti(IV), although these complexes will be characterized by absorptions that are LMCT as opposed to MLCT in character]. Cu(I)-based photosensitizers have their own problems, among them a propensity toward large geometric distortions in the MLCT excited state (which deleteriously affects thermodynamic as well as kinetic factors relevant for photoinduced charge separation), smaller absorption cross sections, and sensitivity to oxygen, but conceptually these compounds have low-energy electronic structures reminiscent of that of $[Ru(bpy)_3]^{2+}$. More recently, progress has been made in using compounds with Ni(II), where long-lived ^{3}MLCT excited states are implicated in photoredox reactions (*21*, *22*); Cr(III) complexes that leverage both electron and energy transfer pathways (*23*, *24*); and a Co(II)-based system that exploits LMCT state reactivity (*25*), to name a few.

Altering the paradigm

Notwithstanding the exciting developments just described, the simple presence or absence of a node in the d-orbital radial distribution function has a substantial influence on what is and is not possible with regard to the photochemistry across the transition block. Whereas this certainly represents a major impediment to the development of scalable approaches to the use of such components for applications of photoinduced electron transfer, it also represents an intriguing fundamental scientific

challenge and, potentially, exciting opportunities for developing new chemistry. At least two different but not mutually exclusive approaches can address these issues. One is the creation of coordination environments that impart sufficiently strong ligand fields to effect the same kind of excited-state inversion found in second- and third-row complexes (this can be done in conjunction with altering the redox potentials of the metal and ligand to shift MLCT state energies). The other is to identify the vibrational degrees of freedom of the compound that couple to excited-state evolution with the goal of redesigning the ligand framework to hinder these degrees of freedom. The first approach is mainly thermodynamic in nature, whereas the second is kinetic.

The potential for success of the first approach is clear from data acquired on $[Fe(bpy)(CN)_4]^{2-}$, in which the lowest-energy excited state appears to be MLCT in nature (*26*). This situation comes about from replacing two of the bpy ligands with the much stronger field afforded by the CN group's ability to act as a strong Lewis acid, which substantially stabilizes the t_{2g} orbitals of the metal center and increases Δ_O.

A more general approach was illustrated in 2013, when Wärnmark and co-workers (*27*) used the strong σ donation properties of an N-heterocyclic carbene ligand to create Fe(II)-based compounds with MLCT excited-state lifetimes on the order of tens of picoseconds; more recent examples have lifetimes of hundreds of picoseconds (*28*). Although this lifetime is still too short to effect bimolecular reaction chemistry under most conditions, this approach nevertheless shows a path forward with the potential for orders-of-magnitude increases in charge-transfer lifetimes by destabilizing the e_g orbitals through strong σ-donor effects. In principle, one could envision amplifying this effect by shifting to higher oxidation states. The resulting photophysical properties would be expected to follow suit. This has now been demonstrated in the context of an LMCT system with Fe(III). By using the same principles that resulted in the extension of MLCT lifetimes for Fe(II) with N-heterocyclic carbenes, Kjær and co-workers have recently reported the first example of an Fe(III) compound that exhibits emission in room-temperature fluid solution (*29*). Steady-state and time-resolved spectroscopies reveal that the state responsible for the emission is ^{2}LMCT in character. These researchers demonstrated that this excited state, which exhibits a lifetime of 2 ns, is both thermodynamically and kinetically competent to engage in bimolecular electron transfer via both oxidative and reductive quenching pathways with methyl viologen and diphenylamine, respectively.

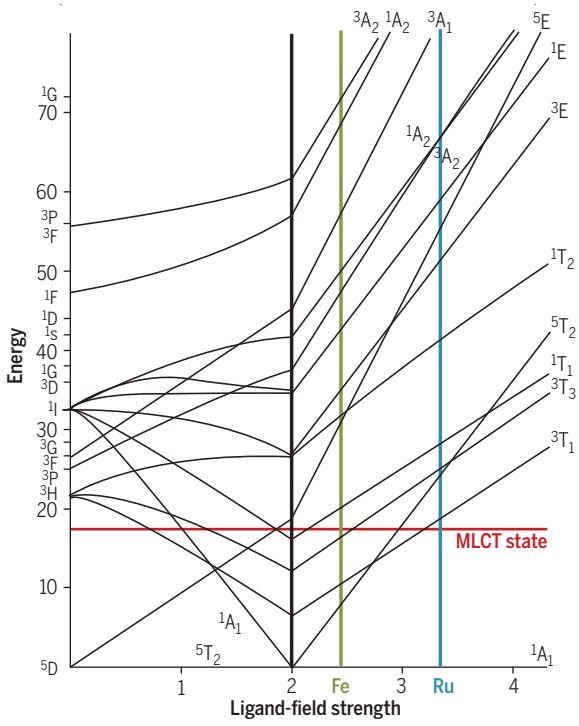

Fig. 4. Relative energetics of excited states. Tanabe-Sugano diagram for a d^6 transition metal complex having pseudo-octahedral symmetry. The red line represents the energy of an MLCT state, whereas the colored vertical lines reflect the relative positions of first- and second-row complexes such as $[Fe(bpy)_3]^{2+}$ (green) and $[Ru(bpy)_3]^{2+}$ (blue), respectively. Letters indicate symmetry.

Identifying the nature of the reaction coordinate that couples to conversion from the charge-transfer to ligand-field manifolds is a less well developed concept at this point but shows considerable promise. This approach takes advantage of the large structural differences that exist between various ligand-field excited states. These large geometric changes are likely to drive the ultrafast nature of MLCT relaxation in the Fe(II)-based chromophores described above, as suggested by Fig. 5. If a subset of the $3N - 6$ vibrational degrees of freedom of a chromophore that define the trajectory of excited-state evolution can be identified, that information could be fed back into synthetic design to modulate the time scale of MLCT state relaxation. In a proof-of-concept experiment in 2010 (*30*, *31*), light pulses of sufficiently short duration (<50 fs) were used to identify vibrational coherence phenomena in the excited-state evolution dynamics of $Cr(acac)_3$ (where acac is the singly deprotonated form of acetylacetone). This compound is not a charge-transfer chromophore—the dynamics involved in this system are strictly within the ligand-field manifold—but a substantial difference in equilibrium geometry exists between the initially formed and lowest-energy excited states of this compound. An analysis of the oscillatory signal (Fig. 6) suggested that the excited-state conversion is coupled to torsional motion of the primary coordination sphere of the molecule. A ligand was redesigned in such a way as to potentially interfere with motion along this trajectory without altering the zero-point energies of the excited states by replacing the terminal CH_3 groups of acac with *tert*-butyl (*t*-Bu) groups to yield $Cr(t\text{-Bu-acac})_3$. This relatively minor (but targeted) structural modification lengthened the time constant for excited-state conversion by roughly two orders of magnitude. Similar experiments on charge-transfer chromophores could identify the modes driving charge-transfer–to–ligand-field conversion, which could then inform synthetic design.

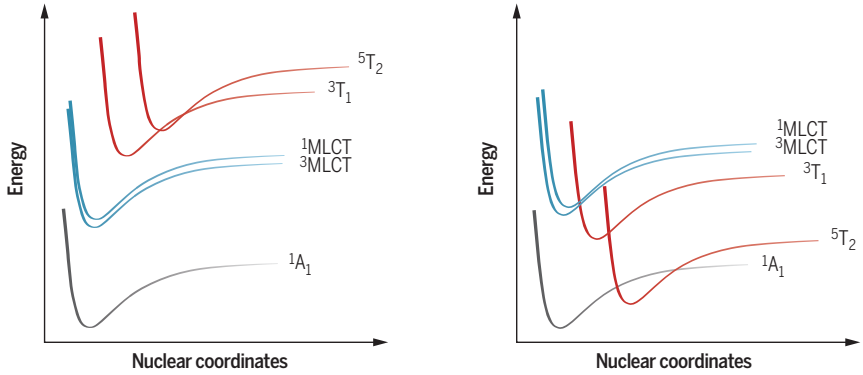

Fig. 5. Comparison of electronic structures. Schematic potential energy surface diagrams appropriate for compounds such as $[Ru(bpy)_3]^{2+}$ (left) and $[Fe(bpy)_3]^{2+}$ (right). Each parabola represents an electronic state corresponding to the energy levels intersected by the colored vertical lines in Fig. 4 (only the two lowest-energy excited ligand-field states are included for clarity). The inversion in the relative energies of the MLCT and ligand-field excited states on going from Ru(II) to Fe(II) is the primary reason for the difference in photophysical behavior between the two classes of compounds.

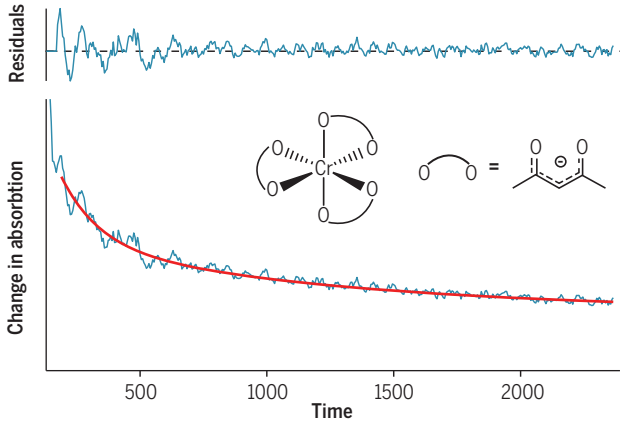

Fig. 6. Re-engineering ligands. Time-resolved absorption data for $Cr(acac)_3$ in CH_3CN solution after excitation into a ligand-field absorption. The oscillations superimposed on the exponential decay kinetics indicated by the red line are due to excited-state coherence, a feature that can be analyzed to afford details concerning the vibrational modes of the molecule that are driving excited-state dynamics. This information can then be used to synthetically redesign the chromophore in the hopes of circumventing the consequences of the primogenic effect discussed in this Review.

Summary and outlook

As noted by Kaupp (*18*), the primogenic effect is something that is familiar to most chemists from atomic theory and is applied widely in the analysis of main group compounds, but it has an underappreciated role in the physical and photophysical properties of transition metal complexes. In the context of the present discussion, this effect is the origin of a fundamental shift in excited-state reactivity of first versus second and third transition series compounds that undermines the ability to use first-row metal complexes as the light absorber for the creation of light-actuated chemical potential. Given this and the recent surge of interest in developing Earth-abundant alternatives for a wide range of chemical processes, it comes as no surprise that substantial effort is being expended to overcome this problem. Although much remains to be done, an understanding of the periodic nature of the problem coupled with the creative work by a growing number of research groups around the world portends that the prospect for a seismic shift in how we interface molecular inorganic chemistry to the science of light capture and conversion is bright indeed.

REFERENCES AND NOTES

1. Intergovernmental Panel on Climate Change, "Global warming of 1.5°C. An IPCC Special Report on the impacts of global warming of 1.5°C above pre-industrial levels and related global greenhouse gas emission pathways, in the context of strengthening the global response to the threat of climate change, sustainable development, and efforts to eradicate poverty," V. Masson-Delmotte, P. Zhai, H. O. Pörtner, D. Roberts, J. Skea, P. R. Shukla, A. Pirani, W. Moufouma-Okia, C. Péan, R. Pidcock, S. Connors, J. B. R. Matthews, Y. Chen, X. Zhou, M. I. Gomis, E. Lonnoy, T. Maycock, M. Tignor, T. Waterfield, Eds. (World Meteorological Organization, 2018).
2. BP, "BP statistical review of world energy" (BP, ed. 67, 2018); https://www.bp.com/en/global/corporate/energy-economics/statistical-review-of-world-energy/downloads.html.
3. A. M. Elshurafa, S. R. Albardi, S. Bigerna, C. A. Bollino, *J. Clean. Prod.* **196**, 122–134 (2018).
4. L. Capuano, "International energy outlook 2018 (IEO2018)" (U.S. Energy Information Administration, 2018).
5. S. Yun *et al.*, *Energy Environ. Sci.* **11**, 476–526 (2018).
6. D. M. Arias-Rotondo, J. K. McCusker, *Chem. Soc. Rev.* **45**, 5803–5820 (2016).
7. S. Ferrere, B. A. Gregg, *J. Am. Chem. Soc.* **120**, 843–844 (1998).
8. N. Sutin, C. Creutz, *Pure Appl. Chem.* **52**, 2717–2738 (1980).
9. A. M. Brown, C. E. McCusker, J. K. McCusker, *Dalton Trans.* **43**, 17635–17646 (2014).
10. J. K. McCusker *et al.*, *J. Am. Chem. Soc.* **115**, 298–307 (1993).
11. J. E. Monat, J. K. McCusker, *J. Am. Chem. Soc.* **122**, 4092–4097 (2000).
12. O. S. Wenger, *J. Am. Chem. Soc.* **140**, 13522–13533 (2018).
13. M. Khalil *et al.*, *J. Phys. Chem. A* **110**, 38–44 (2006).
14. W. Zhang, K. J. Gaffney, *Acc. Chem. Res.* **48**, 1140–1148 (2015).
15. W. Gawelda *et al.*, *J. Am. Chem. Soc.* **129**, 8199–8206 (2007).
16. A. L. Smeigh, M. Creelman, R. A. Mathies, J. K. McCusker, *J. Am. Chem. Soc.* **130**, 14105–14107 (2008).
17. P. Pyykkö, *Chem. Rev.* **88**, 563–594 (1988).
18. M. Kaupp, *J. Comput. Chem.* **28**, 320–325 (2007).
19. A. C. Hernandez-Perez, S. K. Collins, *Acc. Chem. Res.* **49**, 1557–1565 (2016).
20. Y. Liu, S.-C. Yiu, C.-L. Ho, W.-Y. Wong, *Coord. Chem. Rev.* **375**, 514–557 (2018).
21. B. J. Shields, B. Kudisch, G. D. Scholes, A. G. Doyle, *J. Am. Chem. Soc.* **140**, 3035–3039 (2018).
22. C.-H. Lim, M. Kudisch, B. Liu, G. M. Miyake, *J. Am. Chem. Soc.* **140**, 7667–7673 (2018).
23. R. F. Higgins *et al.*, *ACS Catal.* **8**, 9216–9225 (2018).
24. L. A. Büldt, O. S. Wenger, *Chem. Sci.* **8**, 7359–7367 (2017).
25. B. D. Ravetz, J. Y. Wang, K. E. Ruhl, T. Rovis, *ACS Catal.* **9**, 200–204 (2019).
26. J. R. Winkler, C. Creutz, N. Sutin, *J. Am. Chem. Soc.* **109**, 3470–3471 (1987).
27. Y. Liu *et al.*, *Chem. Commun.* **49**, 6412–6414 (2013).
28. P. Chábera *et al.*, *J. Phys. Chem. Lett.* **9**, 459–463 (2018).
29. K. S. Kjær *et al.*, *Science* **363**, 249–253 (2019).
30. J. N. Schrauben, K. L. Dillman, W. F. Beck, J. K. McCusker, *Chem. Sci.* **1**, 405 (2010).
31. G. D. Scholes *et al.*, *Nature* **543**, 647–656 (2017).
32. T. Lu, F. Chen, *J. Comput. Chem.* **33**, 580–592 (2012).

ACKNOWLEDGMENTS

I thank B. Paulus for the data presented in Fig. 6 and B. Paulus and S. Adelman for assistance in the creation of Fig. 3 [by using open source code from (*32*)] and Figs. 5 and 6, as well as H. B. Gray for fruitful discussions. **Funding:** Research related to the topic of this paper that has been carried out in my laboratory has been generously supported by the Chemical Sciences, Geosciences, and Biosciences Division, Office of Basic Energy Sciences, Office of Science, U.S. Department of Energy (grant no. DE-FG02-01ER15282). **Competing interests:** The author declares no competing interests.

10.1126/science.aav9104